THE EFFECTS OF SOLAR FLARES ON SINGLE EVENT UPSET RATES

James H. Adams, Jr.* and Andrew Gelman*

ABSTRACT

Solar flare particle events pose the most extreme SEU producing environment. The most severe aspects of several flares have been combined to produce a model for a composite worst-case flare particle event. This model is proposed as a standard for the design of spacecraft that must operate without interruption.

1. INTRODUCTION

Solar flare particle events can dominate the radiation environment in the interplanetary medium and will affect any spacecraft not well protected by the magnetosphere of the earth or some other planet. These particle events should be a benchmark for the design of spacecraft that must operate all the time and a design consideration for other spacecraft that must recover gracefully from their effects.

In this paper, several large flares have been examined. Using these events as models, a composite worst-case particle event was constructed. The effects of this event on various electronic components within a spacecraft are examined as a function of device sensitivity, spacecraft orbit, and material shielding.

2. SOLAR FLARE PARTICLE EVENTS

Many solar flares are known to give rise to particle radiation enhancements that are observable at earth. A few times a year, these particle events are large enough to dominate the radiation environment in the interplanetary medium near earth. These large events are at their worst for only a few hours, but they may last for a few days.

The data base on large solar flare particle events is sparse. The earliest evidence comes from reports of aurorae, some so large that they could be seen at the equator. Such aurorae may have resulted from gigantic solar flare particle events. The first direct evidence for solar flare particles came from ground-based measurements in the 1940's and 1950's that detected some large events. The heavy ions in solar flare particle events are the principal cause of SEU's. Data on the differential energy spectra of heavy ions in solar flares has only been collected in recent years. However, good data on solar flare proton fluxes has been collected since the mid-1950's. We will use the proton energy spectra to construct a composite of the worst features of the most severe flares. We will then assume that this composite flare is heavy ion rich and use the heavy ion to proton ratios of ref. 8 to get the heavy ion spectra.

The data base on solar flare particle events has recently been reviewed by ref. 1. Figure 1 presents the event integrated proton fluences for all the large flares from 1955 to 1982. Three distinct cycles of solar activity can be seen in the smoothed sunspot numbers. These three cycles are repeated in the frequency distribution of solar flare particle events. The character of the particle events in the three cycles are quite different. The cycle-averaged proton flux of the 19th cycle (1955-1961) exceeds that of the 20th (1966-1972) and 21st (1978-1982) cycles by factors of 4 and 6 respectively. Also the largest flares of the 19th cycle are larger and have harder spectra than those of the later cycles.

*E.O. Hulburt Center for Space Research, Naval Research Laboratory, Washington, D.C. 20375.

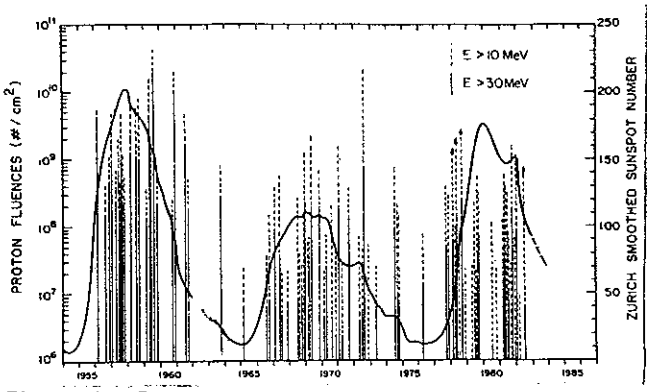

Figure 1: Proton fluences above 10 and 30 MeV in solar flare events during solar-cycles 19, 20, and 21. The solid curve represents Zurich smoothed sunspot numbers.

Of the various flares summarized in figure 1, the events of Feburary 23, 1956, May 10, 1959, July 14, 1959, and Nov. 12, 1960, stand out as the most severe at energies above 30 MeV. Figure 1, however, shows the event-integrated fluence. The most extreme environment occurs at the peak of the flare particle

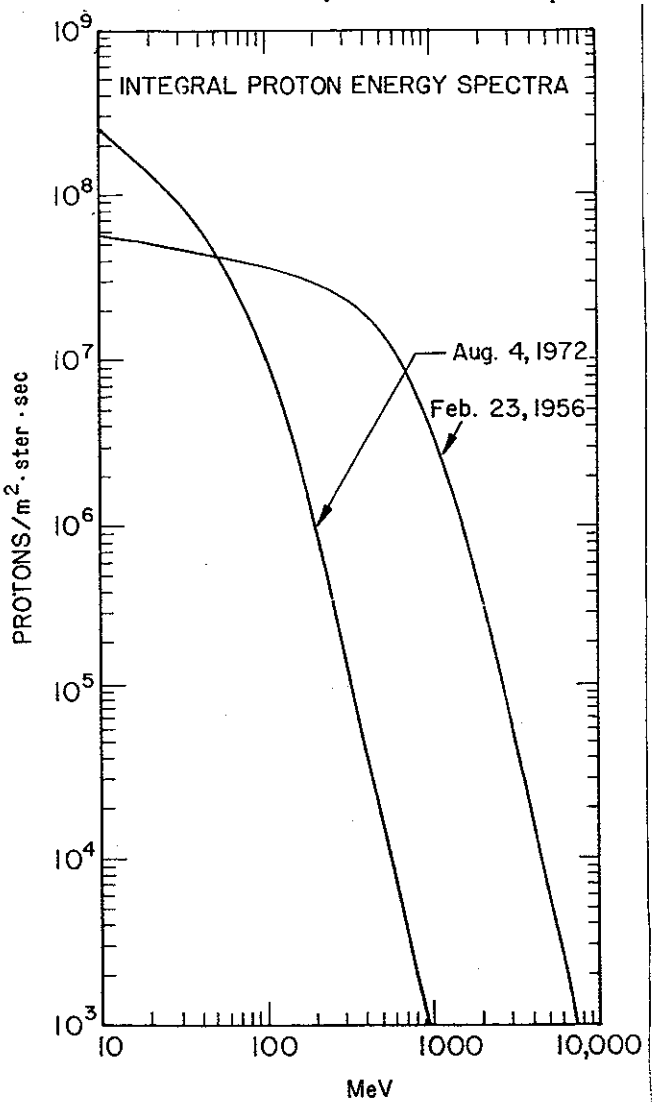

Figure 2: The integral proton energy spectra for the peaks of solar flare particle events of August 4, 1972 and Feburary 23, 1956.

event. The proton differential and integral energy spectra at the peak of these and other flares were examined[2-8]. It was found that the integral proton spectra of all the other flares fell within an upper bound set by the combined integral spectra of the Feb. 23, 1956, event, using the upper bound reported by ref. 4 and the model of the Aug. 4, 1972, flare reported by ref. 8. These two integral proton spectra are shown in figure 2.

Figure 3 shows the proton differential energy spectrum[8] for the solar flare particle event of August 4, 1972. This event is widely used as a benchmark in the radiation effects community. The total radiation dose it delivered was perhaps the most severe of any flare, especially the dose to solar panels. Also shown in figure 3 is the spectrum of the composite formed from the Aug. 4, 1972, and Feb. 23, 1956, flares. It can be seen that the earlier flare was much more intense at high energies. This means that the composite spectrum will penetrate shielding more effectively and produce more SEU's, in most cases, than the event of August 1972 alone.

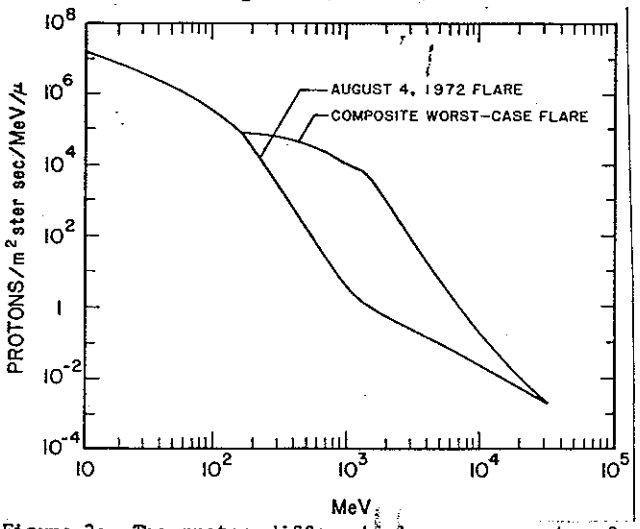

Figure 3: The proton differential energy spectra for the peaks of the August 4, 1972 solar flare particle event and the composite worst-case solar flare particle event.

To complete the description of this composite event, we will assume that it is enriched in heavy ions such that only 10% of all flares are richer in heavy ions than assumed for this composite event. The heavy ion to proton ratios for all the heavy ions through nickel are given in ref. 8. The ratios for the remaining elements to protons were obtained from ref. 9 and enriched, using the procedure in ref. 10. This composite event represents a credible worst-case solar flare particle event at earth for producing SEU's and is proposed as a standard for use in SEU rate calculations.

3. INTEGRAL LET SPECTRA

Most of the SEU's resulting from solar flares are caused by intensely ionizing particles. In this case, integral LET spectra are used to calculate the SEU rate. These spectra present the flux of particles that have an LET greater than or equal to the threshold value. This LET threshold corresponds, in a crude way, to a device SEU threshold, and so the particle flux above the LET threshold is approximately proportional to an SEU rate. With this in mind, LET spectra can be compared directly to get an idea of the relative upset rates for the same device in various environments. Figure 4 shows the LET spectra for the composite worst-case flare behind four thicknesses of shielding. While material shielding does reduce the SEU rate for any device in this environment, the reduction is not as great as reported for the Aug. 4, 1972, event alone[11].

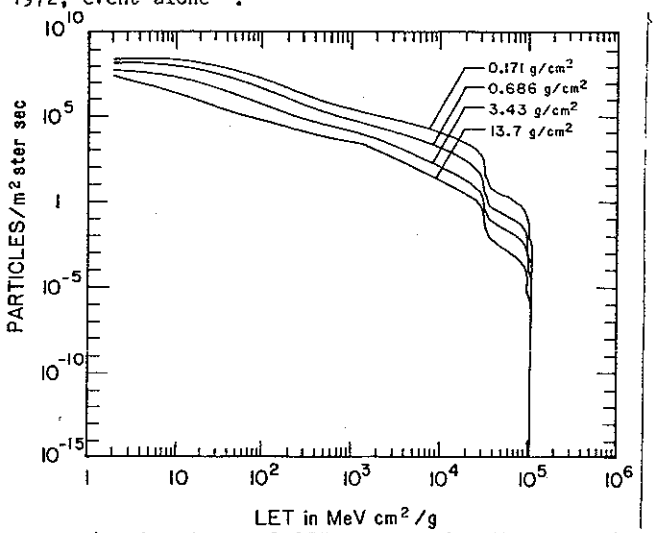

Figure 4: The integral LET spectra for the composite worst-case solar flare particle event outside the magnetosphere. These spectra are behind aluminum shielding of the indicated thicknesses. These thicknesses correspond to 0.025, 0.1, 0.5 and 2.0 inches of aluminum.

These integral LET spectra are also given in table 1. Since each doubling of the shielding thickness causes approximately the same fractional reduction in the LET spectrum, interpolation between spectra is reasonably reliable. These tabulated spectra can be used to compute SEU rates using the method described in ref. 11 for shielding thicknesses between 0.025 and 2.0 inches of alumunum. The approximate effects of other shielding materials can be found by using their equivalent thickness in mass per unit area of aluminum for interpolation in table 1.

Table 1 also contains the integral LET spectrum for the 10% worst-case environment in the interplanetary medium[8]. This environment is constructed such that the instantaneous radiation environment is more severe only 10% of the time.

The effects of geomagnetic shielding on the composite worst-case flare are explored in figure 5. In each case, the integral LET spectrum is behind 0.1 inches of aluminum shielding and the solar flare heavy ions are assumed to be fully ionized. Curve a is the integral LET spectrum outside the magnetosphere. Curves b, c, d, e, and f are the orbit-averaged LET spectra for orbital inclinations of 90, 60, 50, 40, and 30 degrees. All the orbits are circular at 400km altitude, but the shadow of the earth on the spacecraft has not been taken into account. The differences between curve a and curves b through f are just due to the orbit-averaged geomagnetic cutoff transmission to the spacecraft.

Geomagnetic shielding appears to be quite effective, however the combined effects of material and geomagnetic shielding must be considered. The reader should refer to fig. 8 of ref. 11 to see the combined effect of magnetic and material shielding. The ability of material shielding to restore the high LET tail to solar flare LET spectra should be just as important as in the case of cosmic rays.

It has been generally assumed that solar flare particle events do not affect the radiation environment for spacecraft in a 30° inclination orbit at low altitude. Curve g shows the LET spectrum behind 0.1 inches of aluminum shielding, averaged around a 30° inclination circular orbit at 400km, for

the 10% worst-case environment[8] in the interplanetary medium. The contribution from trapped protons[14] is also included. Comparing curves f and g, we see that the composite worst-case flare produces a large increase over the worst radiation environment normally expected in this orbit. The size of this difference above 1000 MeV cm^2/g depends on the validity of the assumption that ultra-heavy nuclei are also enhanced in heavy ion rich solar flares.

TABLE 1: INTEGRAL LET SPECTRA OUTSIDE THE MAGNETOSPHERE

PARTICLE FLUX
(particles/sq. meter ster. sec)

LET (MeV cm^2/g)	10% WORST-CASE * 0.1	* 0.025	COMPOSITE WORST-CASE FLARE * 0.1	* 0.5	* 2.0
1.61E+0	6.32E+3	2.75E+8	1.54E+8	6.29E+7	2.89E+7
2.51E+0	1.86E+3	2.58E+8	1.37E+8	4.74E+7	1.64E+7
3.92E+0	1.26E+3	2.47E+8	1.26E+8	3.68E+7	8.31E+6
6.12E+0	1.12E+3	2.36E+8	1.16E+8	2.95E+7	4.39E+6
9.56E+0	7.49E+2	2.10E+8	9.41E+7	1.91E+7	2.20E+6
1.49E+1	5.37E+2	1.68E+8	6.46E+7	1.01E+7	9.71E+5
2.33E+1	3.40E+2	1.16E+8	3.66E+7	4.84E+6	4.20E+5
3.64E+1	1.92E+2	6.56E+7	1.78E+7	2.17E+6	1.89E+5
5.68E+1	1.09E+2	3.23E+7	8.04E+6	9.40E+5	9.34E+4
8.87E+1	5.90E+1	1.43E+7	3.40E+6	3.97E+5	5.15E+4
1.39E+2	3.06E+1	5.98E+6	1.37E+6	1.70E+5	2.86E+4
1.55E+2	2.65E+1	4.77E+6	1.09E+6	1.38E+5	2.45E+4
1.73E+2	2.29E+1	3.77E+6	8.58E+5	1.12E+5	2.11E+4
1.93E+2	1.97E+1	3.00E+6	6.85E+5	9.18E+4	1.78E+4
2.16E+2	1.73E+1	2.36E+6	5.44E+5	7.54E+4	1.54E+4
2.42E+2	1.54E+1	1.88E+6	4.37E+5	6.28E+4	1.34E+4
2.70E+2	1.28E+1	1.48E+6	3.51E+5	5.20E+4	1.14E+4
3.02E+2	1.12E+1	1.19E+6	2.86E+5	4.36E+4	9.85E+3
3.38E+2	9.58E+0	9.40E+5	2.31E+5	3.64E+4	8.54E+3
3.77E+2	7.97E+0	7.61E+5	1.91E+5	3.05E+4	7.23E+3
4.22E+2	6.86E+0	6.12E+5	1.56E+5	2.56E+4	6.18E+3
4.72E+2	5.84E+0	4.86E+5	1.26E+5	2.13E+4	5.22E+3
5.27E+2	5.06E+0	3.77E+5	1.01E+5	1.76E+4	4.41E+3
5.89E+2	4.46E+0	3.32E+5	8.75E+4	1.53E+4	3.81E+3
6.59E+2	3.96E+0	2.93E+5	7.61E+4	1.33E+4	3.31E+3
7.36E+2	3.47E+0	2.60E+5	6.63E+4	1.17E+4	2.91E+3
8.23E+2	3.11E+0	2.30E+5	5.79E+4	1.04E+4	2.60E+3
9.20E+2	2.74E+0	2.03E+5	5.02E+4	9.35E+3	2.35E+3
1.03E+3	2.43E+0	1.80E+5	4.38E+4	8.49E+3	2.16E+3
1.15E+3	2.14E+0	1.58E+5	3.81E+4	7.78E+3	2.00E+3
1.29E+3	1.38E+0	1.38E+5	3.22E+4	6.41E+3	1.58E+3
1.44E+3	1.03E+0	1.20E+5	2.70E+4	5.21E+3	1.20E+3
1.61E+3	7.90E-1	1.01E+5	2.19E+4	4.13E+3	9.27E+2
1.80E+3	6.10E-1	8.95E+4	1.86E+4	3.31E+3	7.21E+2
2.01E+3	4.68E-1	7.88E+4	1.57E+4	2.61E+3	5.56E+2
2.24E+3	3.60E-1	6.93E+4	1.32E+4	2.05E+3	4.28E+2
2.51E+3	2.78E-1	6.05E+4	1.10E+4	1.61E+3	3.31E+2
2.80E+3	2.15E-1	5.29E+4	9.28E+3	1.27E+3	2.58E+2
3.13E+3	1.66E-1	4.63E+4	7.79E+3	9.92E+2	1.98E+2
3.50E+3	1.27E-1	4.02E+4	6.52E+3	7.67E+2	1.52E+2
3.91E+3	9.87E-2	3.50E+4	5.49E+3	6.03E+2	1.18E+2
4.38E+3	7.63E-2	3.03E+4	4.60E+3	4.72E+2	9.20E+1
4.89E+3	5.85E-2	2.59E+4	3.79E+3	3.65E+2	7.07E+1
5.47E+3	4.48E-2	2.20E+4	3.10E+3	2.83E+2	5.47E+1
6.11E+3	3.45E-2	1.86E+4	2.50E+3	2.19E+2	4.22E+1
6.83E+3	2.63E-2	1.55E+4	1.99E+3	1.68E+2	3.23E+1
7.64E+3	1.95E-2	1.24E+4	1.51E+3	1.25E+2	2.41E+1
8.54E+3	1.50E-2	1.03E+4	1.21E+3	9.75E+1	1.86E+1
9.54E+3	1.13E-2	8.35E+3	9.31E+2	7.39E+1	1.40E+1
1.07E+4	8.42E-3	6.71E+3	7.19E+2	5.65E+1	1.07E+1
1.19E+4	6.15E-3	5.27E+3	5.44E+2	4.29E+1	7.99E+0
1.33E+4	4.43E-3	4.09E+3	4.08E+2	3.22E+1	5.94E+0
1.49E+4	3.12E-3	3.06E+3	2.96E+2	2.36E+1	4.30E+0
1.67E+4	2.24E-3	2.28E+3	2.14E+2	1.72E+1	3.09E+0
1.86E+4	1.60E-3	1.72E+3	1.58E+2	1.26E+1	2.26E+0
2.08E+4	1.08E-3	1.24E+3	1.12E+2	8.88E+0	1.59E+0
2.33E+4	6.64E-4	8.41E+2	7.45E+1	5.91E+0	1.05E+0
2.60E+4	3.25E-4	4.80E+2	4.21E+1	3.35E+0	5.91E-1
2.91E+4	1.46E-5	2.81E+1	2.51E+0	2.83E-1	3.66E-2
3.25E+4	9.18E-7	6.59E+0	6.02E-1	9.75E-2	8.32E-3
3.63E+4	4.78E-7	4.17E+0	3.66E-1	6.42E-2	4.77E-3
4.06E+4	3.12E-7	3.20E+0	2.69E-1	4.69E-2	3.32E-3
4.54E+4	2.00E-7	2.53E+0	2.04E-1	3.48E-2	2.39E-3
5.07E+4	1.30E-7	2.00E+0	1.55E-1	2.56E-2	1.72E-3
5.67E+4	7.87E-8	1.48E+0	1.11E-1	1.81E-2	1.18E-3
6.34E+4	4.33E-8	1.02E+0	7.36E-2	1.19E-2	7.45E-4
7.08E+4	2.47E-8	7.18E-1	4.99E-2	7.83E-3	4.85E-4
7.92E+4	1.25E-8	4.46E-1	2.98E-2	4.56E-3	2.80E-4
8.85E+4	3.50E-9	1.32E-1	8.52E-3	1.32E-3	7.93E-5
9.90E+4	2.27E-10	4.34E-3	2.73E-4	4.74E-5	2.65E-6

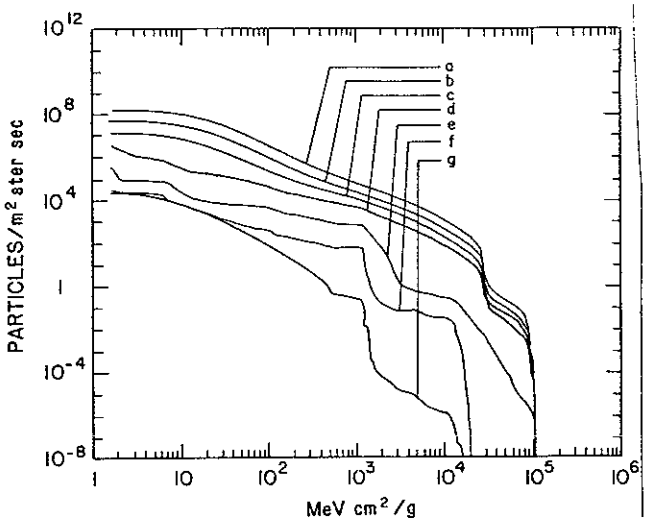

Figure 5: The integral LET spectra for various circular orbits at 400km altitude. Curves b, c, d, e, and f are orbit-averaged LET spectra due to the composite worst-case solar flare for orbital inclinations of 90, 60, 50, 40, and 30 degrees respectively. Curve a is the LET spectrum for the worst-case solar flare outside the magnetosphere. Curve g is the orbit-averaged LET spectrum for a 30° inclination circular orbit at 400 km and a 10% worst-case environment in the interplanetary medium. All spectra are behind 0.1 inches of aluminum and solar flare heavy ions are assumed to be fully ionized.

4. SEU RATES FOR TYPICAL DEVICES

SEU rates in the composite worst-case flare environment have been computed for three typical devices. The model data for the 93422 and the HM6508RH were taken from ref. 13, while the model data for a N-MOS d-RAM was taken from ref. 12.

Table 2: DEVICE PARAMETERS

PART NO.	DIMENSIONS OF THE CRITICAL VOLUME (in micrometers)	CRITICAL CHARGE (in picocoulombs)
93422	30X30X2	0.014
N-MOS d-RAM	21X14X3.5	0.249
HM6508RH	20X15X2.2	0.82

Figure 6 compares the SEU rates for these devices outside the earth's magnetosphere as a function of aluminum shielding. The solid curves are for the composite worst-case flare, while the dashed curves are for the environment of the Aug. 4, 1972, event. It is clear from this figure that using the Aug. 4 event as a model would lead to an overestimate of the effectiveness of shielding.

Figure 7 shows how the orbit-averaged SEU rates would vary for these devices as a function of orbital inclination for circular orbits at 400 km altitude. The devices are assumed to be behind 100 mils of aluminum shielding and the heavy ions from the solar flare are assumed to be fully ionized as they enter the magnetosphere. The reader is cautioned that the charge state of solar flare heavy ions is not known, though they are often assumed to be fully ionized. It should also be noted that the instantaneous SEU rate will vary around the orbit.

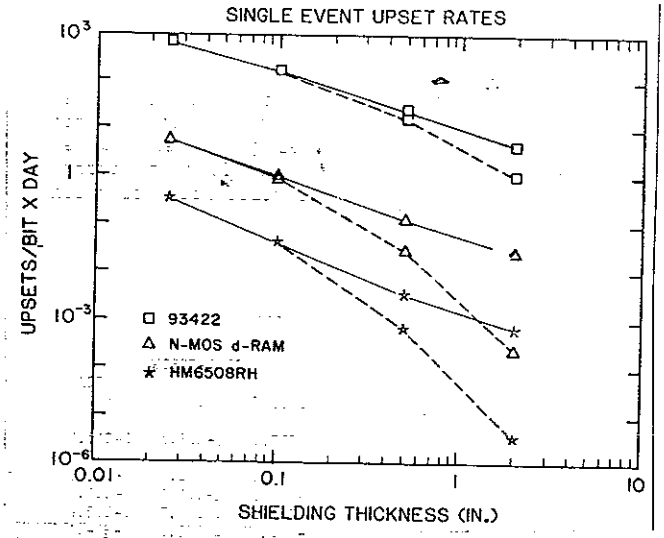

Figure 6: Single event upset rates for three devices as a function of the thickness of aluminum shielding in inches. The solid curve is for the composite worst-case solar flare particle event and the dashed curve is for the August 4, 1972 solar flare particle event.

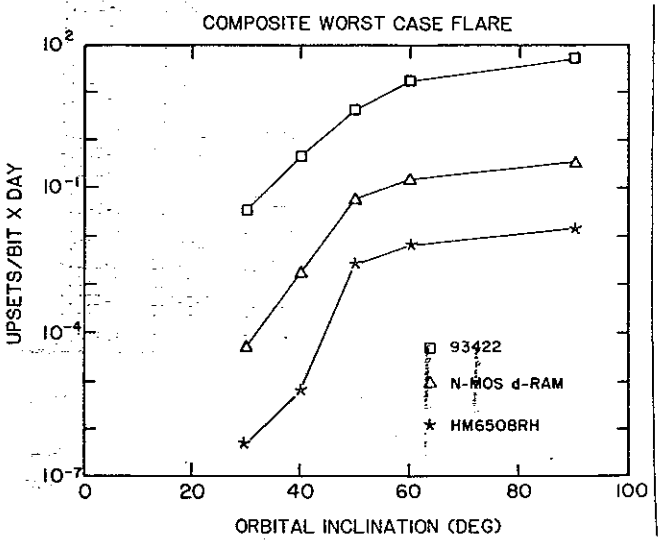

Figure 7: Orbit-averaged single event upset rates for three devices as a function of orbital inclination for the composite worst-case solar flare environment. All orbits are circular and 400km altitude. All the devices are assumed to be shielded by 0.1 inches of aluminum.

5. CONCLUSIONS

The composite worst-case flare environment presented here is a credible worst-case flare particle environment, based on all the available data. It represents the sort of SEU producing environment that spacecraft must tolerate if they have to operate without interuption. Material shielding is effective in moderating the solar flare particle environment. The effectiveness of geomagnetic shielding depends on the charge state of solar flare heavy ions. A conservative design assumption at present would be to neglect the benefits of geomagnetic shielding. If geomagnetic shielding effects are included, the effects of the material shielding present in the spacecraft must also be considered. It should also be remembered that the upset rates presented in figure 7 are orbit-averaged. The actual rate will vary around the orbit. For the higher inclination orbits, the instantaneous rate will approach the rate outside the magnetosphere at some points in the orbit.

The composite solar flare particle environment is far more severe than the one normally present (see ref. 11) in space, even for low altitude and low inclination orbits. The composite solar flare particle environment imposes an extreme demand on spacecraft design. A critical factor determining the cost and complexity of spacecraft electronic systems is the willingness of the spacecraft manager to tolerate ocassional outages. If 99% "up" time is acceptable, then no large solar flares have to be tolerated and a much milder environment can be specified for the spacecraft design considerations.

6. ACKNOWLEDGEMENTS

This research was partially supported by NAVELEX under the Nuclear Survivability/Vulnerability Program and Defense Nuclear Agency under the Subtask X99QMXBA, Work Unit 00018/Single Event Program.

7. REFERENCES

1. R. E. McGuire, J. N. Goswami, R. Jha, D. Lal and R. C. Reedy, "Solar Flare Particle Fluences During Solar Cycles 19, 20, and 21",18th Intl. Cosmic Ray Conference, Vol. 4, p. 66-69, Bangalore, India, 1983.

2. T. W. Armstrong, R. G. Alsmiller, Jr. and J. Barish, "Calculation of the Radiation Hazard at Supersonic Aircraft Altitudes Produced by an Energetic Solar Flare", Nuclear Science and Engineering, Vol. 37, p. 337-342 (1969).

3. P. S. Freier and W. R. Webber, "Exponential Rigidity Spectrums for Solar Flare Cosmic Rays", JGR, vol. 68, 1605-1629 (1963).

4. Trutz Foelsche, "The Ionizing Radiations in Supersonic Transport Flights", Proc. of the Second Symp. on Protection Against Radiation in Space, 287-299, Gatlinburg, Tennessee, Oct. 12-14, 1964.

5. R. R. Brown and R. G. D'Arcy, "Observations of Solar Flare Radiation at High Latitude During The Period July 10-17, 1959", Phys. Rev. Letters, vol. 3, 390-2 (1959).

6. R.C. Reedy and J. R. Arnold, "Interaction of Solar and Galactic Cosmic-Ray Particles with the Moon", JGR, vol. 77, 537-555 (1972).

7. M. O. Burrell, "The Risk of Solar Proton Events to Space Missions", NASA TN D-6379, Marshall Space Flight Center (1971).

8. J. H. Adams, Jr., R. Silberberg, and C. H. Tsao, "Cosmic Ray Effects on Microelectronics, Part I: The Near-Earth Particle Environment", NRL Memorandum Report 4506, August 25, 1981.

9. A. G. W. Cameron, "Elementary and Nuclidic Abundances in the Solar System", Havard-Smithsonian Center for Astrophysics Preprint Series No. 1357 (1980).

10. W. F. Dietrich and J. A. Simpson, "Preferential Enhancements of the Solar Flare Accelerated Nuclei Carbon to Zinc from 20-300 MeV/nucleon", Ap. J., vol. 225, L41-45 (1978).

11. James H. Adams, Jr., "The Variability of Single Event Upset Rates in the Natural Environment", IEEE Trans. on Nuclear Science, vol. NS-30, 4475-4480 (1983).

12. P. Shapiro, E. L. Petersen, and J. H. Adams, Jr., "Calculation of Cosmic-Ray Induced Soft Upsets and Scaling in VLSI Devices", NRL Memorandum Report 4864, Aug. 26, 1982.

13. E. L. Petersen, J. B. Langworthy, and S. E. Diehl, "Suggested Single Event Upset Figure of Merit", IEEE Trans. on Nucl. Sci., vol. 30, 4533-4539, (1983).

14. E.G. Stassinopoulos and J.M. Barth, "Non-Equatorial Terrestrial Low Altitude Charged Particle Radiation Environment", NASA-X-601-82-9, Goddard Space Flight Center, March, 1982.